IEEE Photonics Journal
An IEEE Photonics Society Publication

Open Access

High-Order Mode Mode-Locked Fiber Laser Based on Few-Mode Saturable Absorber

Volume 13, Number 3, June 2021

Yi Huang
Si Lv
Linping Teng
Longtao Wang
Jiafeng Lu
Jiangtao Xu
Xianglong Zeng

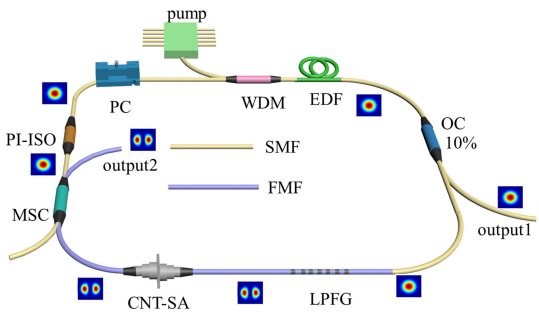

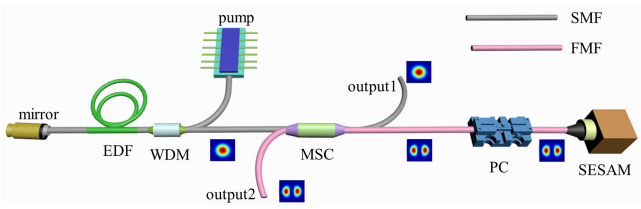

DOI: 10.1109/JPHOT.2021.3077571

High-Order Mode Mode-Locked Fiber Laser Based on Few-Mode Saturable Absorber

Yi Huang, Si Lv, Linping Teng, Longtao Wang, Jiafeng Lu, Jiangtao Xu, and Xianglong Zeng

Key Laboratory of Specialty Fiber Optics and Optical Access Networks, Joint International Research Laboratory of Specialty Fiber Optics and Advanced Communication, Shanghai Institute for Advanced Communication and Data Science, Shanghai University, Shanghai 200444, China

DOI:10.1109/JPHOT.2021.3077571

Manuscript received March 31, 2021; revised April 19, 2021; accepted April 29, 2021. Date of publication May 4, 2021; date of current version June 1, 2021. This work was supported in part by the Science and Technology Commission of Shanghai Municipality (STCSM) under Grant 20JC1415700, and by the Open Research Fund of State Key Laboratory of Pulsed Power Laser Technology (SKL2020KF03) and 111 Project (D20031). The work of Xianglong Zeng the support of the Program for Professor of Special Appointment (Eastern Scholar) at Shanghai Institutions of Higher Learning. Corresponding author: Xianglong Zeng (e-mail: zenglong@shu.edu.cn).

Abstract: We presented two kinds of high-order mode (HOM) mode-locked fiber lasers based on few-mode (FM) saturable absorbers for direct HOM oscillation. One is a ring fiber laser based on a carbon nanotube (CNT) saturable absorber (SA), in which the combination of a long period fiber grating (LPFG) and a mode selective coupler (MSC) is used for the cycle of mode conversion between LP_{01} and LP_{11} modes. The other is a linear-cavity laser using a FM-based SESAM with the HOM oscillation, in which a MSC is used for mode conversion inside the cavity. The presented mode-locked fiber lasers can achieve the saturable absorption of the HOM and the cylindrical vector beams (CVBs). And we also compared the nonlinear saturation absorption characteristics of two SAs operating at LP_{01} and LP_{11} modes.

Index Terms: Long period fiber grating, mode selective coupler, nonlinear saturation absorption characteristic, high-order mode mode-locked fiber laser.

1. Introduction

The Mode division multiplexing (MDM) technology based on few-mode fiber (FMF) solves the problem of insufficient capacity of single-mode fiber (SMF) communication system [1]–[4]. Therefore, MDM technology has attracted the attention of researchers. Compared with the fundamental mode of SMF, the high-order modes (HOMs) in FMF have a special electromagnetic field distribution. The degenerate linear polarization mode is made up of different vector eigenmodes, which can excite orbital angular momentums (OAMs). They are widely used in optical micromachining [5], remote sensing [6], quantum entanglement and other fields [7], [8]. The methods of generating HOM are reported in many ways, such as laterally offset-splicing technique [9], photonic lantern [10], fiber Bragg grating (FBG) [11], LPFG [12]–[14], acoustically induced fiber grating (AIFG) and mode selective coupler (MSC) [15]–[20]. These technologies are relatively mature, and there have been many reports on the generation of HOMs in fiber lasers. Despite the fact that most of

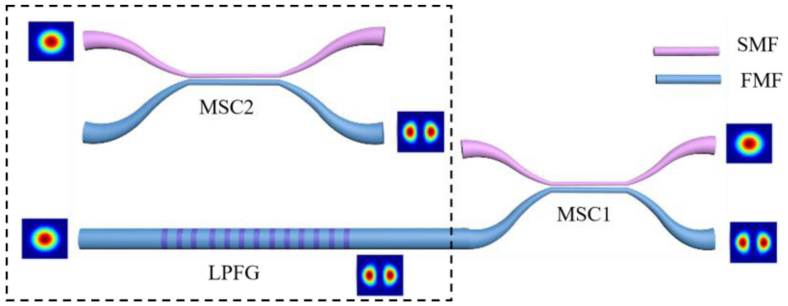

Fig. 1. Schematic of cascaded LPFG and MSC through FMF ports.

mode-locked lasers generate higher-order modes outside of the cavity, the fundamental mode is still oscillating inside the cavity [21]–[23].

Compared with SMF lasers, multiple transverse modes in FMF lasers become interesting due to the unique polarization and amplitude distribution. L. G. Wright *et al*. demonstrated the concept of spatiotemporal mode-locking in multimode fiber lasers, in which longitudinal modes and transverse modes in multi-mode fiber are locked simultaneously [24]. This provides further guidance for temporal locking of transverse modes. Wang *et al*. achieved LP_{11} mode oscillation in all-FMF lasers for the first time, but only Q-switched pulses could be obtained [25]. Chen *et al*. achieved an all-FMF laser to generate a mode-locked spectrum with a 3-dB bandwidth of 0.33 nm [26]. The direct oscillation of HOM in FMF lasers provides a research platform for multimode non-linear propagation, high power fiber lasers, random lasers [27], [28].

In this paper, two kinds of SAs, CNT and FM-based SESAM are used to form mode-locked HOMs based on ring and linear hybrid cavities of SMF and FMF, respectively. The MSC and LPFG are used inside the laser cavity to generate LP_{11} mode. The contrast of the mode converters at 1550 nm is greater than 15 dB (the corresponding conversion efficiency is more than 97%). The LP_{11} mode in the cavities will directly oscillate and be mode locked by using the FM-based SAs. The output spectra of the ring cavity and the linear-cavity lasers have 3-dB bandwidth of 6.6 nm and 5 nm, respectively. In addition, the nonlinear saturation absorption characteristics of two SAs with LP_{01} and LP_{11} modes are measured, which proves that the nonlinear absorption characteristics of LP_{11} mode are similar to those of LP_{01} mode. We proved that mode-locked HOMs in half SMF and half FMF cavities directly oscillate and generate LP_{11} mode and CVBs, and LP_{11} modal light can be saturably absorbed by CNT-SA and FM-based SESAM.

2. Fabrication and Characterization of Mode Converters

In order to realize the oscillation of LP_{11} mode in the hybrid laser cavity, a cascaded structure of LPFG and MSC1 is proposed as shown in Fig. 1. The incident LP_{01} mode firstly is converted to LP_{11} mode by the LPFG, which is connected to the FMF of the MSC1. According to the reversibility of the MSC1, the converted LP_{11} mode input from the FMF of MSC1 can be reconverted into LP_{01} mode at the SMF of MSC1. The LP_{11} mode without mode conversion would be output at the FMF of the MSC1. The same result can be obtained by replacing the LPFG with the MSC2. The LP_{11} modal light will directly inject into the SA inserted between these two devices. The CO_2-laser glass processing system (LZM-100) is used to fabricate LPFG by point-by-point exposure process. The heating source is a highly stable CO_2 laser, and the output spot energy presents a Gaussian distribution. The fabrication of the LPFG is roughly divided into two steps: laser irradiation and moving motor. In addition, the axial stress is applied by the small displacement difference between the left and right motors, and the distance of the motor movement is the period of the LPFG. In order to monitor the transmission spectrum of LPFG during real-time writing process, a segment of SMF is spliced at both ports of the FMF, the light from the broadband source is injected into the

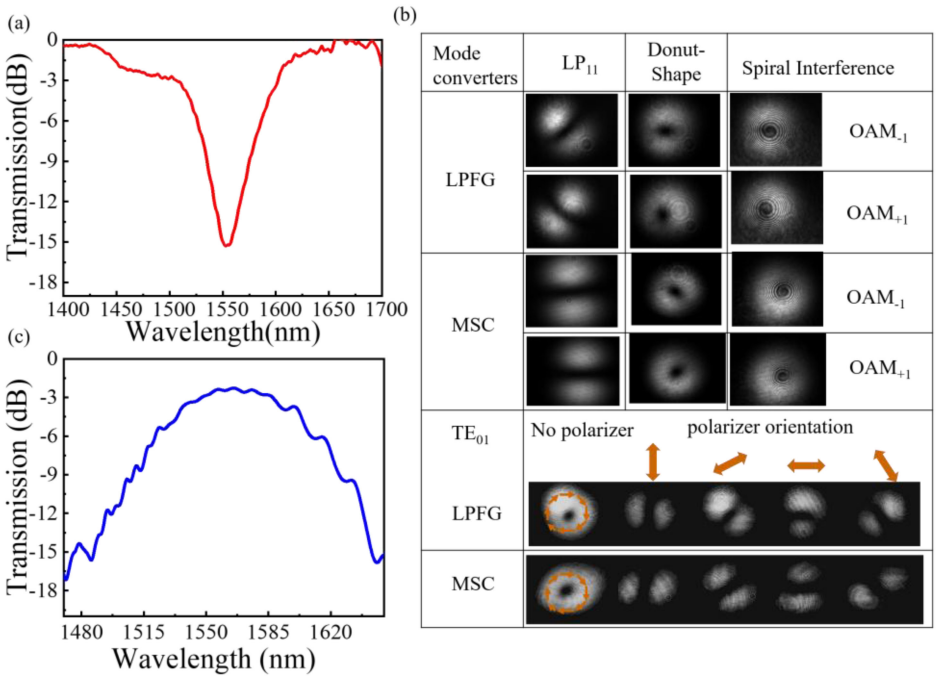

Fig. 2. (a) Transmission spectrum of LPFG operating at 1.5 μm. (b) Intensity distribution of LP_{11} mode, donut-shape OAMs, spiral interferences and the spatial distribution of TE_{01} from LPFG and MSC. (c) The transmission spectrum of cascading LPFG and MSC.

FMF and the LPFG is connected to an optical spectrum analyzer (OSA) to monitor the transmission spectrum. The mode strippers are placed on each side of the FMF to ensure that only LP_{01} mode is launched into the LPFG and detected at the output port. According to the coupled-mode theory, the phase matching condition of the LPFG can be given as [14]

$$\Lambda = \lambda_{res}/(n_{eff,01} - n_{eff,11}) \tag{1}$$

where Λ is the period of the grating, λ_{res} is the resonance wavelength, $n_{eff,01}$ and $n_{eff,11}$ are the effective indices of the LP_{01} mode and LP_{11} mode, respectively. In the experiment, the cladding and core diameters of the FMF are 125 μm and 20 μm, respectively, and the refractive index difference is 0.5% between the core and the cladding of the fiber. The FMF supports four modes, including LP_{01}, LP_{11}, LP_{21} and LP_{02} modes. The period of the LPFG is about 1210 μm, and the transmission spectrum of LPFG is shown in Fig. 2(a). It can be seen that the contrast at the resonance wavelength of 1550 nm is greater than 15 dB, and the conversion efficiency is about 97%.

The fusion taper technology is applied in the fabrication of the MSC. SMF and FMF are stretched and fused together by using the Oxyhydrogen flame. The output ports of SMF and FMF are detected by power meters, respectively. According to the coupled-mode theory [29], the power of SMF and FMF in MSC can be defined as

$$|A(z)|^2 = 1 - k\sin^2(Dz) \tag{2}$$

$$|B(z)|^2 = k\sin^2(Dz) \tag{3}$$

Where $A(z)$ and $B(z)$ represent the slowly-varying field amplitudes of the mode in SMF and FMF, respectively, z is the coupling length, and D is defined as $D = c/\sqrt{k}$. The power transfer coefficient

k is given by

$$k \approx \left[1 + \frac{(\beta_A - \beta_B)^2}{4c^2}\right]^{-1} \tag{4}$$

When the propagation constants of different modes in two fibers are equal ($\beta_A = \beta_B$) which means the effective index of the LP_{01} mode in the SMF is equal to that of the LP_{11} mode in the FMF, their power in two fibers can be converted, LP_{01} mode in the SMF will be coupled to LP_{11} mode in the FMF. By pre-tapering the fiber to change its diameter, the propagation constants of different modes can be changed. Therefore, SMF has to be pre-tapered to a specific diameter to satisfy the phase matching condition, and then stretch and fuse FMF and SMF together. When stretched to a certain length, LP_{01} mode in the SMF would be coupled to the LP_{11} mode in the FMF, and the power in the FMF reaches the maximum. In the experiment, SMF is selected as Corning SMF-28e fiber. The same FMFs are used in the MSC and the LPFG. When the SMF diameter is pre-tapered to 78 μm, the LP_{01} mode in the SMF can be well coupled into the LP_{11} mode in the FMF. The MSC has a contrast of 20 dB and the insert loss below 1 dB at 1550 nm (the corresponding conversion efficiency is 99%). The conversion bandwidth at 10-dB can exceed 200 nm and the transmission spectrum of the MSC can refer to the previous result [30].

The mode field distributions of LPFG and MSC mode converters at the FMF output port are detected by using a near-IR CCD (charge-coupled device). As shown in Fig. 2(b), LP_{11} mode with two-lobe-shaped intensity patterns can be observed. By adjusting the PC, different vector eigenmodes can be excited in both mode converters, and the OAM with first-order topology charges can be obtained. A polarizer is used to testify the vector polarization of the donut-shaped beams, showing that the output ports at the LPFG and MSC are azimuthally polarized beam (TE_{01} mode). The transmission spectrum of the cascaded structure of LPFG and MSC is also measured as shown in Fig. 2(c). The transmission spectrum is still relatively wide, and the insertion loss around 1550 nm is less than 3 dB.

3. HOM Mode-Locked Laser Based on FM Saturable Absorber

Combining two kinds of mode converters (LPFG and MSC) with mode-locking techniques in the hybrid fiber laser, we have achieved direct oscillation and mode locking of the LP_{11} mode. In the ring cavity, the CNT is used to realize the saturable absorption of the LP_{11} mode. The LPFG and the MSC are connected to achieve the oscillation of LP_{11} mode inside the cavity. In the linear-cavity, the saturable absorption of the LP_{11} mode is realized by the FM-based SESAM. The MSC acts as the cycle of mode conversion between LP_{01} and LP_{11} modes.

3.1 HOM Mode-Locked Laser Based on CNT-SA

In the experiment, CNT-SA is inserted between the LPFG and the MSC, and the LP_{11} mode generated by the LPFG is directly mode-locked by CNT-SA [31]. The experimental setup is shown in Fig. 3(a). The laser consists of a 980/1550 nm wavelength division multiplexer (WDM), a length of 0.5 m erbium-doped fiber (EDF), a LPFG, a MSC, a 10% optical coupler (OC) and a polarization independent isolator (PI-ISO). The OC is used to extract the energy of the laser and can be connected to an OSA to monitor the mode-locking state of the laser. The LP_{11} mode generated by LPFG oscillates in the FMF of the cavity, and the mode field distribution of output2 is recorded by CCD camera to verify the oscillation of the LP_{11} mode inside the cavity. In addition, a typical balanced twin-detector measurement technology is used to measure the nonlinear absorption characteristics of the CNT operating at LP_{01} and LP_{11} modes, as shown in Fig. 3(b). It can be seen that the red and blue curves have similar change trends, which indicates that the nonlinear absorption characteristics of the CNT operating at the LP_{11} mode are similar to these operating at the LP_{01} mode. The modulation depth of the CNT can be fitted as [32]

$$T(I) = 1 - \Delta T \exp(-I/I_{sat}) - T_{ns} \tag{5}$$

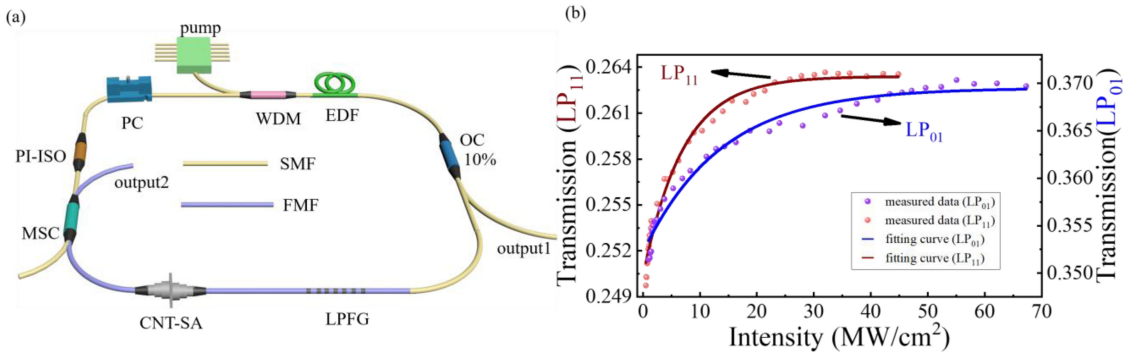

Fig. 3. (a) Schematic of ring cavity laser. (b) Nonlinear saturable absorption of CNT-SA.

where T is the transmission, ΔT is the modulation depth, I is the incident light intensity, I_{sat} is the saturable intensity and T_{ns} is the nonsaturable absorption. The fitting result shows that the modulation depth of the CNT operating at the LP_{01} mode is 1.7%, while the modulation depth of the CNT is 1.3% for LP_{11} mode. The transmission of the CNT in the LP_{11} mode is smaller than that in the LP_{01} mode. The reason may be that the light field intensity of the LP_{01} mode is Gaussian distribution and light energy is mainly concentrated in the core area, while the LP_{11} mode has two-lobe-shaped intensity patterns, and its effective mode field area is larger than that of LP_{01} mode. Moreover, part of LP_{01} modal light could interfere with LP_{11} modal light in the FMF.

The cavity loss can be adjusted by a PC to achieve mode locking. The output spectrum from output1 is recorded by an OSA as shown in Fig. 4(a). A broadband spectrum with Kelly sideband is observed, which is a typical spectrum of traditional soliton in anomalous dispersion cavity. And the center wavelength of the laser is 1560 nm with a 3-dB bandwidth of 6.6 nm. The time domain characteristic of the laser is measured by an oscilloscope, as shown in Fig. 4(b), the repetition frequency of the pulse train is 20.3 MHz. Simultaneously, the radio frequency analyzer can measure the signal to noise ratio of the laser as 65 dB, as shown in Fig. 4(c). This indicates that the laser is working at a stable mode-locked state. The mode field distribution from output2 is measured by a CCD camera to prove the oscillation and the saturable absorption of the LP_{11} mode in the laser cavity. The LP_{11} mode can be observed. The FMF at the output2 is squeezed and rotated by a PC, so that a certain vector mode with the maximum coupling efficiency can be obtained to eliminate the degeneracy of the LP_{11} mode, and finally the donut-shaped mode patterns can be achieved. A polarizer is placed between the FMF of the output2 and the CCD camera. The rotation of the polarizer realizes two-lobe-shaped intensity patterns in different directions. As shown in Fig. 4(d), it represents the TE_{01} mode when the mode field intensity distribution is perpendicular to the direction of the polarizer and the TM_{01} mode when the mode field intensity distribution is the same as the direction of the polarizer. The generation of the HOM mode-locked pulse verifies the saturable absorption of the LP_{11} mode by using the CNT-SA. Since the effective mode area of the LP_{11} mode is larger than that of the LP_{01} mode, the CNT-SA has a low transmittance for the LP_{11} mode, and the reverse conversion efficiency of the MSC is lower than the forward conversion efficiency.

3.2 HOM Mode-Locked Fiber Laser Based on FM- Based SESAM

The experimental setup of the half SMF and half FMF linear-cavity based on FM-based SESAM is shown in Fig. 5(a). The laser consists of a 980/1550 nm WDM, a length of 0.4 m EDF, a MSC, a mirror and a FM-based SESAM. The WDM is connected with the EDF for gain amplification of the LP_{01} mode. The FM-based SESAM is used to achieve the saturable absorption of LP_{11} modal light and acts as a mirror. The LP_{01} mode is reflected back into the cavity by the mirror and then converted to the LP_{11} mode by the MSC. LP_{11} mode in the FMF is injected into the

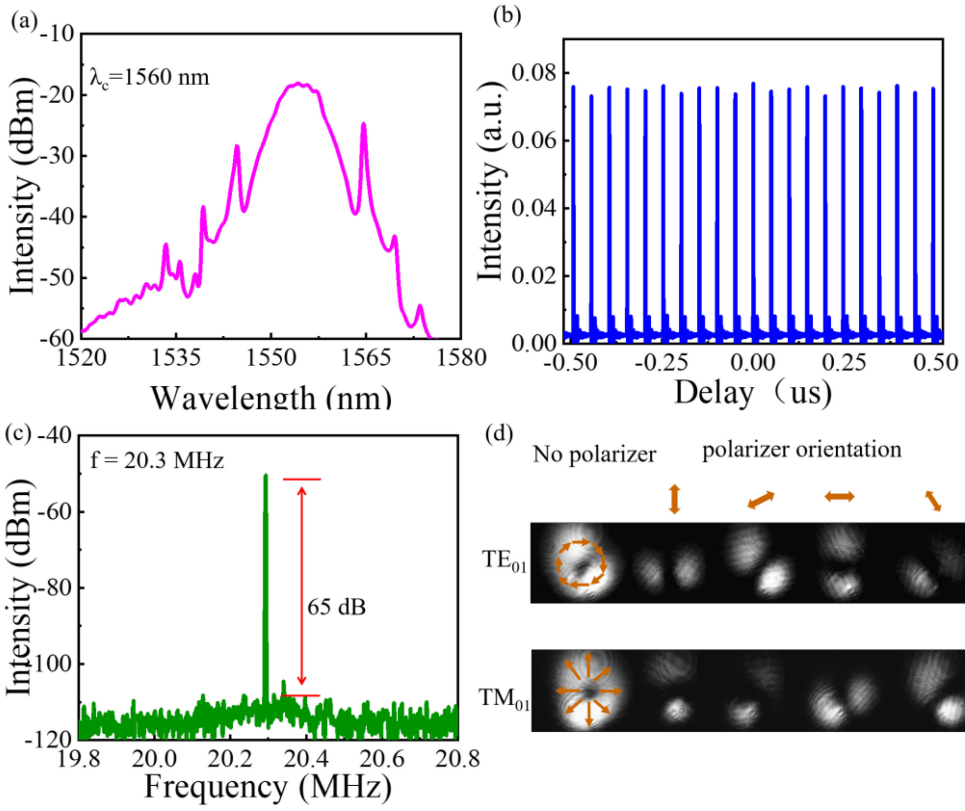

Fig. 4. (a) Output spectrum of ring cavity laser. (b) Typical mode-locked pulse train. (c) Radio frequency of pulse. (d) The spatial distribution of TE_{01} and TM_{01} modes.

FM-based SESAM and reflected back into the cavity, and then reconverted to LP_{01} mode by the MSC. Therefore, the output1 port of MSC can be used to extract the energy in the cavity to monitor the mode-locking state of the laser. The intensity distribution of the output2 port of the laser can be recorded by CCD camera to verify the oscillation of the LP_{11} mode inside the cavity. For the FM-based SESAM, the nonlinear absorption characteristics in the cases of LP_{01} and LP_{11} are also measured by the balanced twin-detector measurement technology. Fig. 5(b) shows the nonlinear transmittance of the SESAM, the green and purple curves represent the fitted curves of the LP_{11} mode and LP_{01} mode, respectively. The similar trend of the two curves indicates that the FM-based SESAM operating at the LP_{11} mode has similar characteristics as operating at LP_{01} mode. The modulation depth of the SESAM is 4.7% in the case of LP_{01} mode, while the modulation depth of the SESAM is 2% in the case of LP_{11} mode.

Self-started mode-locking occurs when the pump power reaches 50 mW. The mode-locked spectrum of a typical traditional soliton with Kelly sideband is shown in Fig. 6(a). The center wavelength is 1558 nm and the 3-dB bandwidth is 5 nm. Fig. 6(b) shows the pulse train and the repetition frequency of the pulse train is 13.89 MHz. At the same time, the SNR measured by radio frequency analyzer is 58 dB, as show in Fig. 6(c). In order to verify the operation of the LP_{11} mode inside the cavity, the mode field distribution of the output2 is monitored by a CCD camera. A PC is used to rotate and squeeze the FMF at the output2 port to generate a phase difference between the different vector modes and remove the degeneracy of the LP_{11} mode. The intensity distribution of the two-lobe-shaped intensity patterns is observed by rotating the polarizer. Fig. 6(d) shows the TE_{01} mode where the mode field intensity distribution direction is perpendicular to the direction of the polarizer and the TM_{01} mode where the mode field intensity distribution direction is consistent

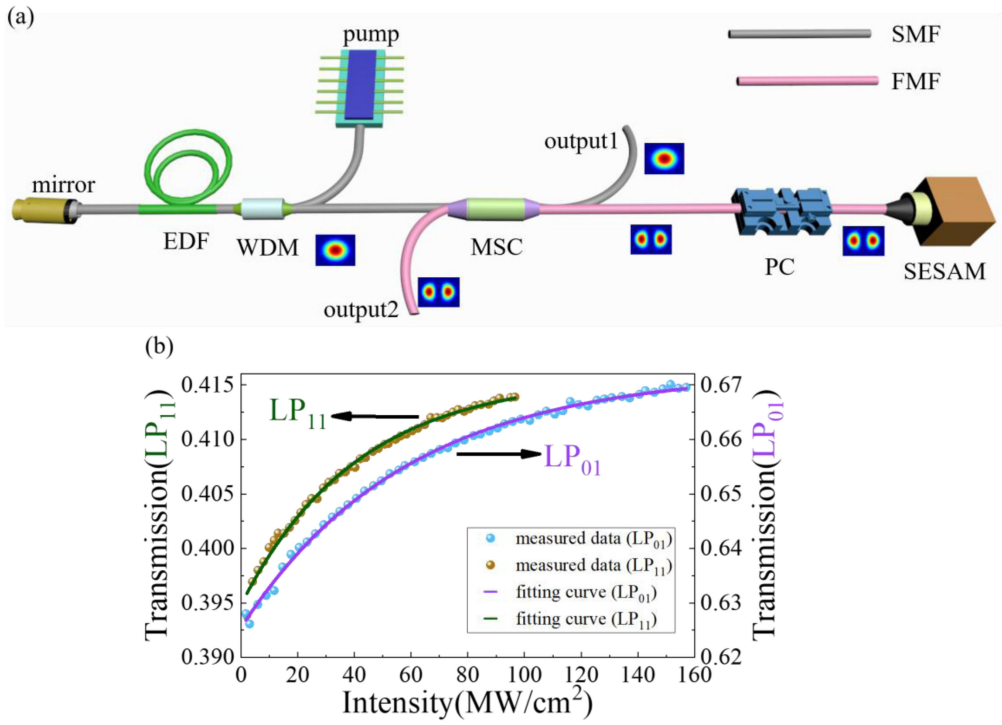

Fig. 5. (a) Schematic of linear-cavity laser. (b) Nonlinear saturable absorption of SESAM.

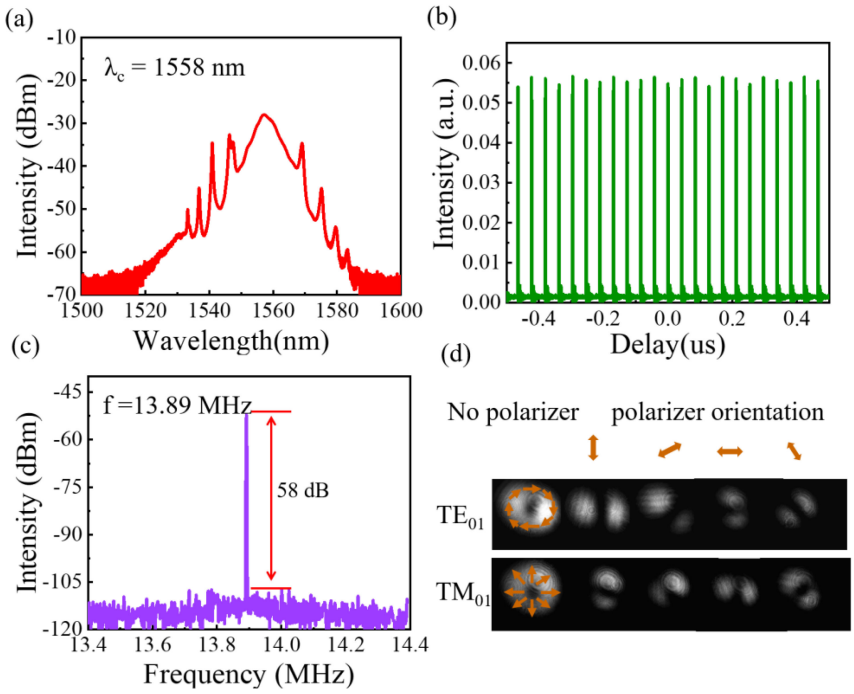

Fig. 6. (a) Output spectrum of linear-cavity laser. (b) Typical mode-locked pulse train. (c) Radio frequency of pulse. (d) The spatial distribution of TE_{01} and TM_{01} modes.

with the direction of the polarizer. Similarly, the generation of the HOM mode-locked pulse verifies the saturable absorption of the LP_{11} mode by using the FM-based SESAM. The reversibility of the MSC is utilized by the linear-cavity, it is worth noting that the reverse conversion efficiency of the MSC is lower than the forward conversion efficiency, resulting in a relatively high loss of the laser cavity.

4. Conclusion

In conclusion, we experimentally provided two methods of directly generating HOM mode-locking pulses in the hybrid laser cavities, which are a ring cavity composed of a CNT-SA and a linear-cavity composed of a FM-based SESAM. In the ring cavity, we use the reversibility of MSC to connect the LPFG with the MSC, and the CNT-SA is inserted between these devices. The LP_{11} mode oscillates inside the cavity, and it can prove the saturable absorption of the LP_{11} mode. In the linear-cavity, the generation of the LP_{11} mode benefits from the broadband MSC, and the experiment also proves the saturable absorption of the LP_{11} mode by using the FM-based SESAM. The LP_{11} mode and CVBs can be generated with two mode-locked laser cavities. In addition, we compared the nonlinear saturation absorption characteristics of the SAs in different modal light and showed that the transmission and modulation depth of two SAs in LP_{11} mode are slightly lower than those in LP_{01} mode. This research is useful for effectively obtaining higher-order modes and cylindrical vector beams in FMF lasers.

References

[1] R.-J Essiambre, G. Kramer, P. J. Winzer, G. J. Foschini, and B. Goebel, "Capacity limits of optical fiber networks," *J. Lightw. Technol.*, vol. 28, no. 4, pp. 662–701, Feb. 2010.

[2] D. J. Richardson, J. M. Fini, and L. E. Nelson, "Space-division multiplexing in optical fibers," *Nat. Photon.*, vol. 7, no. 5, pp. 354–362, 2013.

[3] N. Bai, E. Ip, T. Wang, and G. Li, "Multimode fiber amplifier with tunable modal gain using a reconfigurable multimode pump," *Opt. Exp.*, vol. 19, no. 17, pp. 16601–16611, 2011.

[4] R. Ryf *et al.*, "Mode-division multiplexing over 96 km of few-mode fiber using coherent 6 × 6 MIMO processing," *J. Lightw. Technol.*, vol. 30, no. 4, pp. 521–531, Feb. 2012.

[5] C. Hnatovsky, V. Shvedov, W. Krolikowski, and A. Rode, "Revealing local field structure of focused ultrashort pulses," *Phys. Rev. Lett.*, vol. 106, no. 12, 2011, Art. no. 123901.

[6] L. Chen, J. Lei, and J. Romero, "Quantum digital spiral imaging," *Light: Sci. Appl.*, vol. 3, 2014, Art. no. e153.

[7] M. Padgett and R. Bowman, "Tweezers with a twist," *Nat. Photon.*, vol. 5, no. 6, pp. 343–348, 2011.

[8] C. Gabriel *et al.*, "Entangling different degrees of freedom by quadrature squeezing cylindrically polarized modes," *Phys. Rev. Lett.*, vol. 106, no. 6, 2011, Art. no. 060502.

[9] Y. Zhou *et al.*, "Actively mode-locked all fiber laser with cylindrical vector beam output," *Opt. Lett.*, vol. 41, no. 3, pp. 548–550, 2016.

[10] S. G. Leon-Saval, A. Argyros, and J. Bland-Hawthorn, "Photonic lanterns," *Nanophotonics*, vol. 2, no. 5, pp. 429–440, 2013.

[11] L. Wang, P. Vaity, B. Ung, Y. Messaddeq, L. A. Rusch, and S. LaRochelle, "Characterization of OAM fibers using fiber Bragg gratings," *Opt. Exp.*, vol. 22, no. 13, pp. 15653–15661, 2014.

[12] J. Dong and K. S. Chiang, "Temperature-insensitive mode converters with CO_2-laser written long-period fiber gratings," *IEEE Photon. Technol. Lett.*, vol. 27, no. 9, pp. 1006–1009, May 2015.

[13] W. Wang, J. Wu, K. Chen, W. Jin, and K. S. Chiang, "Ultra-broadband mode converters based on length-apodized long-period waveguide gratings," *Opt. Exp.*, vol. 25, no. 13, pp. 14341–14350, 2017.

[14] Y. Zhao, Y. Liu, L. Zhang, C. Zhang, J. Wen, and T. Wang, "Mode converter based on the long-period fiber gratings written in the two-mode fiber," *Opt. Exp.*, vol. 24, no. 6, pp. 6186–6195, 2016.

[15] L. Meng *et al.*, "Multi-orthogonal high-order mode converter based on acoustically Induced fiber gratings," *IEEE Photon. Technol. Lett.*, vol. 32, no. 13, pp. 819–822, Jul. 2020.

[16] J. Lu *et al.*, "Dynamic mode-switchable optical vortex beams using acousto-optic mode converter," *Opt. Lett.*, vol. 43, no. 23, pp. 5841–5844, 2018.

[17] W. Zhang *et al.*, "High-order optical vortex generation in a few-mode fiber via cascaded acoustically driven vector mode conversion," *Opt. Lett.*, vol. 41, no. 21, pp. 5082–5085, 2016.

[18] D. R. Song, H. S. Park, B. Y. Kim, and K. Y. Song, "Acoustooptic generation and characterization of the higher order modes in a four-mode fiber for mode-division multiplexed transmission," *J. Lightw. Technol.*, vol. 32, no. 23, pp. 4534–4538, Dec. 2014.

[19] J. D. Love and N. Riesen, "Mode-selective couplers for few-mode optical fiber networks," *Opt. Lett.*, vol. 37, no. 19, pp. 3990–3992, 2012.

[20] K. Y. Song, I. K. Hwang, S. H. Yun, and B. Y. Kim, "High performance fused-type mode-selective coupler using elliptical core two-mode fiber at 1550 nm," *IEEE Photon. Technol. Lett.*, vol. 14, no. 4, pp. 501–503, Apr. 2002.
[21] J. Dong and K. S. Chiang, "Mode-locked fiber laser with transverse-mode selection based on a two-mode FBG," *IEEE Photon. Technol. Lett.*, vol. 26, no.17, pp. 1766–1769, Sep. 2014.
[22] Y. Huang *et al.*, "High-order mode Yb-doped fiber lasers based on mode-selective couplers," *Opt. Exp.*, vol. 26, no. 15, pp. 19171–19181, 2018.
[23] F. Wang, F. Shi, T. Wang, F. Pang, T. Wang, and X. Zeng, "Method of generating femtosecond cylindrical vector beams using broadband mode converter," *IEEE Photon. Technol. Lett.*, vol. 29, no. 9, pp. 747–750, May 2017.
[24] L. G. Wright, D. N. Christodoulides, and F. W. Wise, "Spatiotemporal mode-locking in multimode fiber lasers," *Science*, vol. 358, no. 6359, pp. 94–97, 2017.
[25] T. Wang *et al.*, "High-order mode direct oscillation of few-mode fiber laser for high-quality cylindrical vector beams," *Opt. Exp.*, vol. 26, no. 9, pp. 11850–11858, 2018.
[26] S. Chen, W. Hu, Y. Xu, Y. Cai, Z. Wang, and Z. Zhang, "Mode-locked pulse generation from an all-FMF ring laser cavity," *Chin. Opt. Lett.*, vol. 17, no. 12, 2019, Art. no. 121405.
[27] C. Jauregui, J. Limpert, and A. Tünnermann, "High-power fiber lasers," *Nat. Photon.*, vol. 7, no. 11, pp. 861–867, 2013.
[28] F. Antenucci, A. Crisanti, M. Ibáñez-Berganza, A. Marruzzo, and L. Leuzzi, "Statistical mechanics models for multimode lasers and random lasers," *Philos. Mag.*, vol. 96, no. 7–9, pp. 704–731, 2016.
[29] N. Riesen and J. D. Love, "Weakly-guiding mode-selective fiber couplers," *IEEE J. Quantum Electron.*, vol. 48, no. 7, pp. 941–945, Jul. 2012.
[30] P. Cheng, F. Shi, L. Meng, T. Wang, F. Pang, and X. Zeng, "All-fiber wavelength-tunable bandpass filter based on core-mode conversion for mode-locking laser," *Opt. Eng.*, vol. 59, no. 9, 2020, Art. no. 096101.
[31] P. Xiao, K. Wu, D. Mao, and J. Chen, "A pulsewidth measurement technology based on carbon-nanotube saturable absorber," *Opt. Exp.*, vol. 27, no. 4, pp. 4188–4203, 2019.
[32] Y. Chen *et al.*, "Mechanically exfoliated black phosphorus as a new saturable absorber for both Q-switching and mode-locking laser operation," *Opt. Exp.*, vol. 23, no. 10, pp. 12823–12833, 2015.